



Supplement of

Can low-resolution CMIP6 ScenarioMIP models provide insight into future European post-tropical-cyclone risk?

Elliott Michael Sainsbury et al.

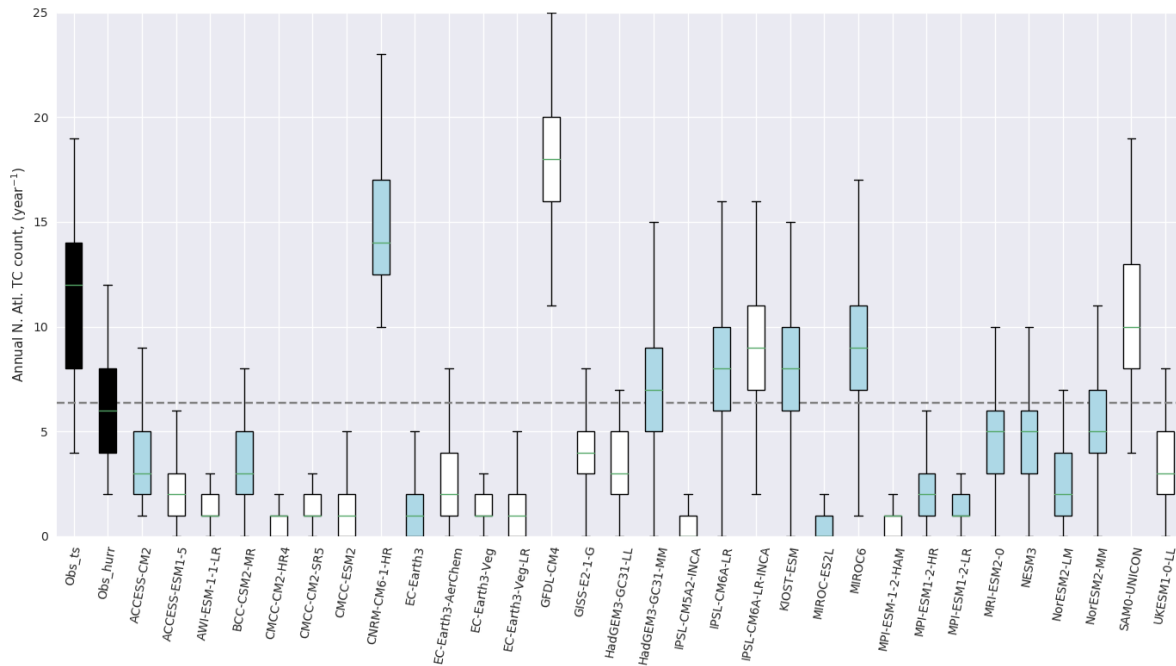
Correspondence to: Elliott Michael Sainsbury (e.sainsbury@pgr.reading.ac.uk)

The copyright of individual parts of the supplement might differ from the article licence.

1 **1. CMIP6 model selection**

2 The CMIP6 models used in the main manuscript were chosen from a large sample of CMIP6 models, based on
 3 their ability to simulate TCs in the North Atlantic. Figure S1 shows boxplots for North Atlantic TC frequency
 4 (hurricane season only), averaged over the entire historical run, for all the considered models. The green lines
 5 show the median, the box contains the interquartile range, and the maxima and minima are shown by the bars
 6 above and below the boxes. Between 1950 and 2014 (HURDAT2), there are approximately 12 TCs per year in
 7 the North Atlantic which have winds more than 17ms^{-1} , and 6.4 hurricanes per year (winds $> 33\text{ms}^{-1}$). These are
 8 labelled ‘Obs_ts’ and ‘Obs_hurr’ in Figure S1 respectively.

9 Based on Figure S1, we select all CMIP6 models which have a median annual North Atlantic TC frequency
 10 greater than the average number of hurricanes per year (6.4) in observations. Boxplots are colored blue if SSP5-
 11 85 scenario data is also available, and white if not. Of the 8 models which have a median TC frequency greater
 12 than 6.4 TCs per year, 5 of these models also have the high-frequency relative vorticity fields needed for
 13 tracking for the SSP5-85 scenario. These models are therefore retained for further analysis.

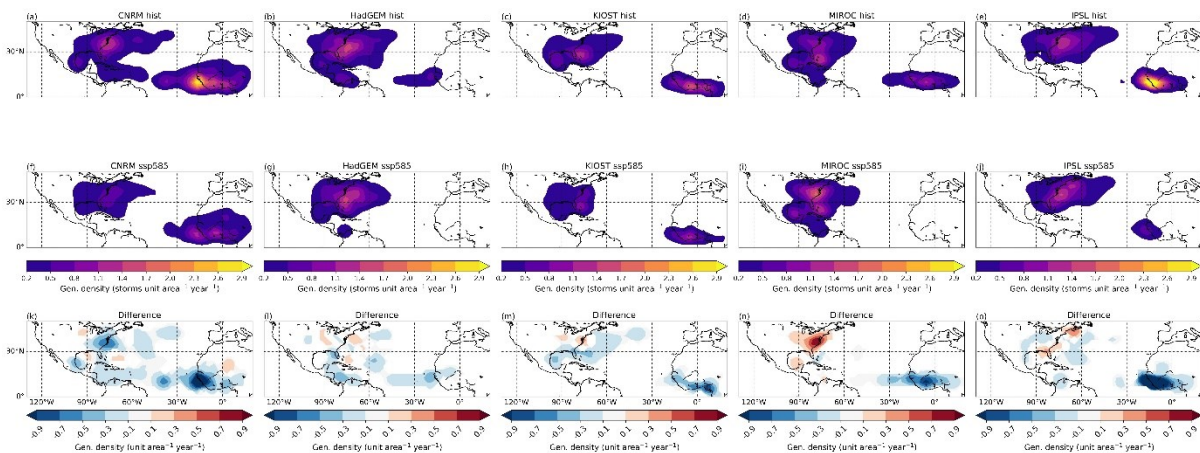


14
 15 **Figure S1: Boxplot showing the North Atlantic TC frequency (June 1st – Nov 30th), averaged over the**
 16 **entire historical run, for a selection of CMIP6 models and HURDAT2 (first two boxes, black). ‘Obs_ts’**
 17 **represents all cyclones present in HURDAT2 with winds $\geq 17\text{ms}^{-1}$. ‘Obs_hurr’ represents all hurricanes**
 18 **(winds $\geq 33\text{ms}^{-1}$) present in HURDAT2. Grey horizontal line represents the threshold of 6.4 TCs per**
 19 **year used to select models for further analysis, which is the average number of hurricanes per year in**
 20 **HURDAT2 between 1950 and 2014. Blue boxes represent models which have sufficient data available for**
 21 **the SSP5-85 scenario to perform cyclone tracking and TC identification, and boxes which are not filled**
 22 **blue do not have sufficient SSP5-85 data available, and so cannot be considered in this study.**

23
 24 **2. TC identification method**

25 Objective TC identification methods such as used in Hodges et al. (2017) identify cyclone tracks as TCs if
 26 (among other things) they have a coherent vertical structure and a warm core, diagnosed using the vertical
 27 profile of relative vorticity. To achieve a balance between hit rate and false alarm rate, a latitude constraint is
 28 imposed such that the TC must have a genesis location equatorward of 30N. In the present climate, this is quite
 29 suitable as most TCs forming in the North Atlantic basin form equatorward of 30N (though there are notable
 30 exceptions, such as Ophelia in 2017). However, climate change may extend the genesis region of TCs further
 31 polewards and eastwards (e.g., Haarsma et al. 2013), and so a 30N threshold may lead to many future TCs being
 32 misidentified as non-tropical by virtue of where they form.

33 Figure S2 shows the genesis density for the 5 CMIP6 models in the historical (1984-2014) and future (2069-99)
 34 periods, along with the differences (future-historical). Here we identify the TCs using criteria in section 2.3,
 35 however criteria 1) has been relaxed to 45N, to investigate whether there is any model consensus for increased
 36 genesis of TC-like features between 30 and 45N. Figure S2 shows no robust increase in TC genesis between 30
 37 and 45N, though there is some increase in the MIROC along the US East Coast. We therefore use a 30N
 38 constraint throughout the main manuscript with confidence that we are not missing a large trend in subtropical
 39 TC genesis poleward of 30N.



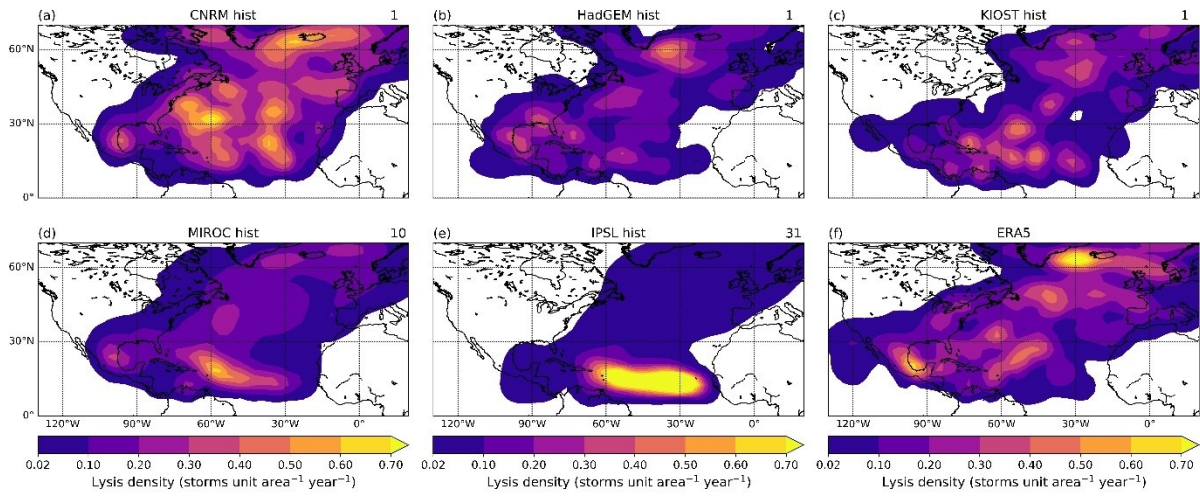
40
 41 **Figure S2: Genesis density for the historical (1984-2014, a-e) and future (2069-99, f-j) periods for the five**
 42 **selected CMIP6 models along with the differences (future-historical, k-o). TCs are identified using the**
 43 **criteria described in section 2.3 of the main manuscript, but the latitude constraint has been relaxed to**
 44 **45N.**

45

46 3. Historical Lysis Density

47 Figures 2 and 4 in the main manuscript indicate that the TCs forming in the main development region in the
 48 IPSL model are weak, short-lived TCs. To investigate this further, a spatial map of the lysis density is created
 49 for the 5 models and ERA5, shown in Figure S3. There is a large region of non-zero lysis densities in the
 50 tropics, subtropics and midlatitudes in all the models and ERA5, highlighting that vast region in which TCs
 51 travel and dissipate. Many models (and ERA5) have their highest (or joint highest) lysis density values in the
 52 subtropics and midlatitudes. However, the IPSL is very different from the other models. In the IPSL, the highest
 53 lysis density values occur in the MDR, very close to where the storms form. These TCs form on the west coast

54 of Africa (Fig. 1), indicating that the storms are dissipating with little opportunity to move from their place of
 55 origin. This further indicates the severe bias in the MDR of the IPSL.

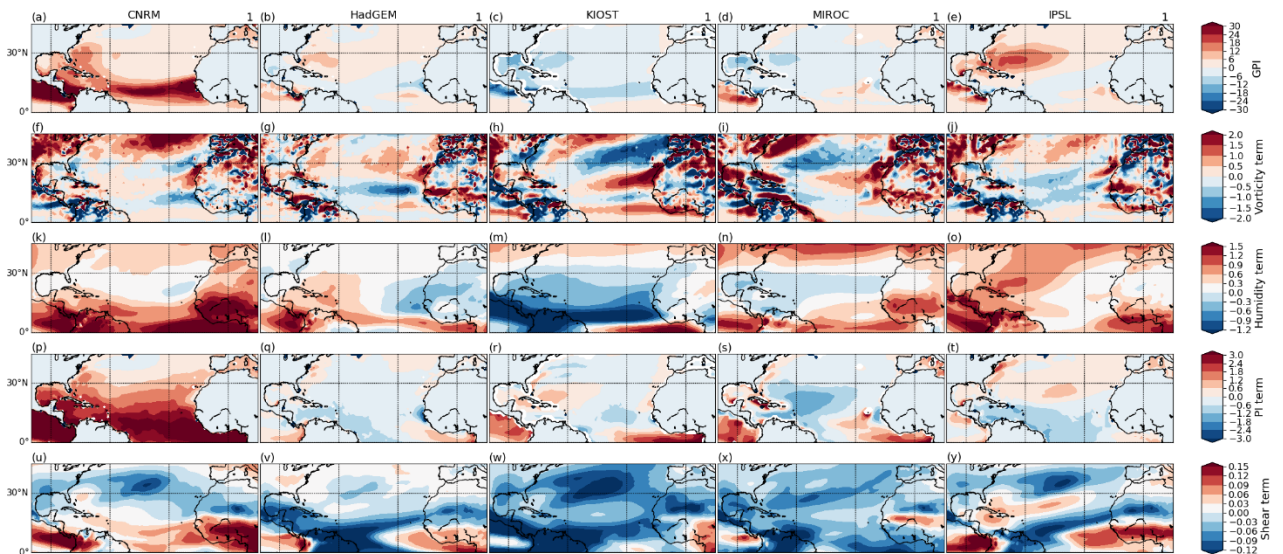


56
 57 **Figure S3: Lysis density (storms per unit area per year, where the unit area is equal to a spherical cap**
 58 **with a 5-degree radius) for the 1984-2015 period from the historical runs of 5 CMIP6 models (a-e) and**
 59 **ERA5 (f). All ensemble members are used where available. Densities less than 0.02 have been masked for**
 60 **clarity.**

61

62 **4. Historical GPI bias**

63 Figure S4 shows the bias in GPI (and individual terms) for the fully historical coupled runs from 1984-2014.
 64 Biases are calculated relative to ERA5. All models except CNRM have a negative GPI bias or no GPI bias (top
 65 row) in the main development region. All models except the CNRM have too much wind shear in the western
 66 MDR, increasing hostility (row 5).



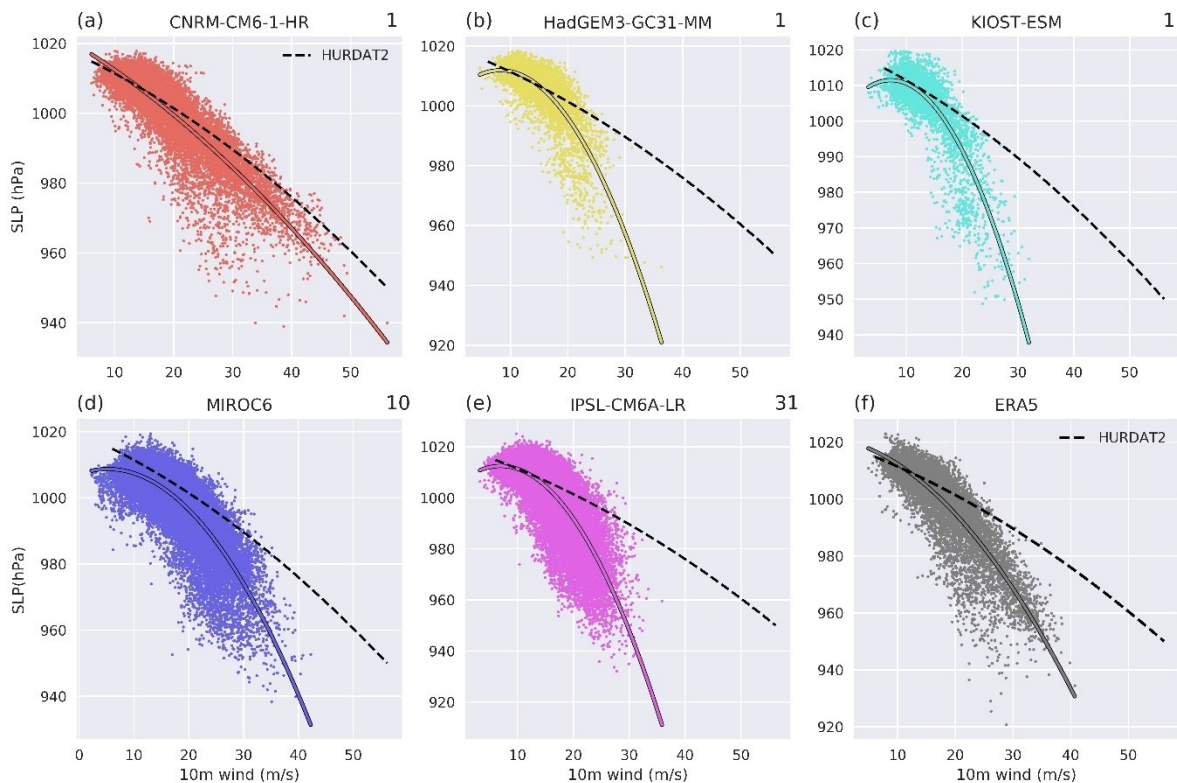
67

68 **Figure S4: Bias (model minus ERA5) in GPI (top row) and the terms comprising GPI (rows 2-5). Data**
69 **from 1984-2014 is used for ERA5 and the fully-coupled historical runs. Note that a positive bias in the**
70 **shear term means a low-bias in wind shear.**

71

72 **5. Wind-pressure relationship**

73 The wind-pressure relationships for the warm-core part of the tracks (i.e., the part of the track at which the
74 criteria in section 2.3 are satisfied) over the historical period is compared with ERA5 and HURDAT2 in Figure
75 S5. The relationship between wind and pressure in TCs is well-established, and using one point for each TC, or
76 all points for each TC, should not change the results. ERA5 and all of the CMIP6 models have a slope which is
77 too steep, where cyclones do not reach the expected (from HURDAT2 observations) wind speeds for a given sea
78 level pressure. The apparent intensity of the TCs is greater in terms of their sea level pressure than in terms of
79 their maximum winds. This result has also been found in other reanalyses in previous studies (Hodges et al.,
80 2017). This difference is smallest for CNRM, which simulates stronger TCs than the other 4 models. Despite
81 this, in all 5 models (and ERA5), there is a clear relationship between wind and pressure in the tropical stage of
82 the identified TCs, a feature present in observed TCs.



83

84 **Figure S5: Wind-pressure relationship for the TCs (during their TC phase) for selected CMIP6 models**
85 **(a-e) and ERA5 (grey, f). Coloured lines on each panel show a quadratic polynomial fit for each CMIP6**
86 **model and ERA5, dashed black line shows the quadratic polynomial fit for HURDAT2. The number of**
87 **ensemble members used for each model is shown to the upper-right of each panel.**

88

89

6. Relationship between TC frequency and recurving TC frequency

90

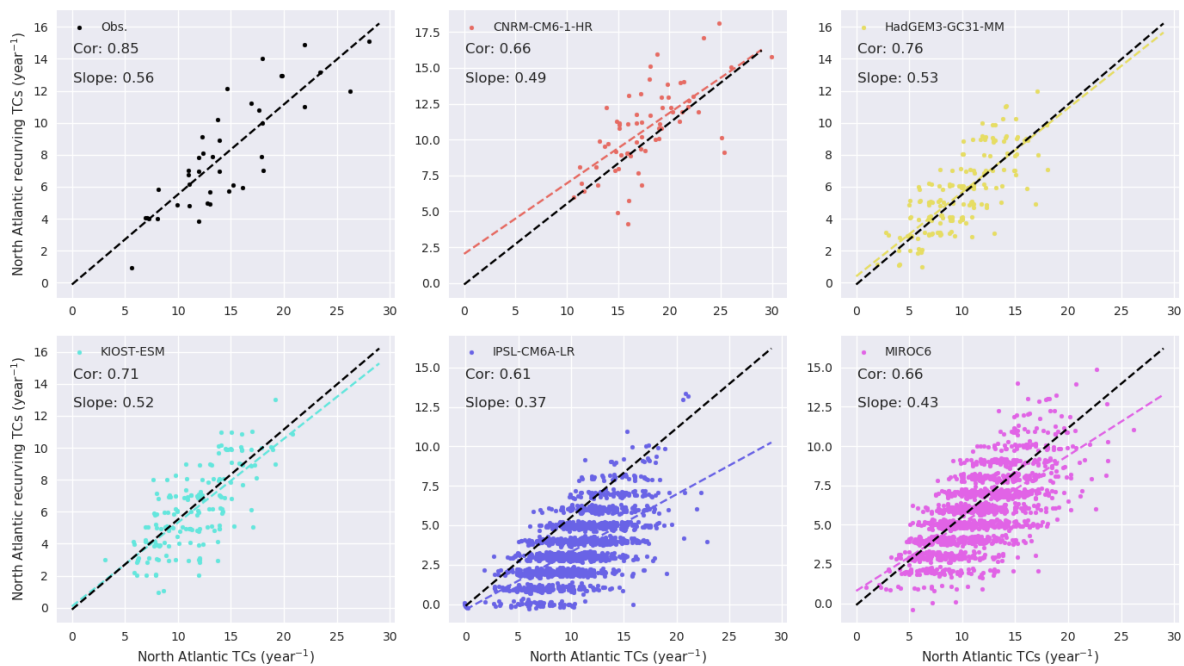
To reach Europe as a PTC, a TC must first interact with the midlatitudes (i.e., enter the ‘recurvature’ domain shown in Figure 1 of the main manuscript). Previous work has shown that there is a strong relationship between TC activity and recurving TC activity (Sainsbury et al., 2022). It is therefore important that CMIP6 models can capture this relationship, as it may have implications for the frequency of Europe-impacting PTCs. The ability of the selected CMIP6 models to capture this relationship is explored in Figure S6. In ERA5 (TCs identified using track matching with HURDAT2), there is a significant relationship between TC frequency and recurving TC frequency (top left panel, $r=0.85$). A strong relationship is also found in the CMIP6 models (correlations 0.61-0.76), which are statistically significant in all cases to the 95% level. CNRM, HadGEM and KIOST all have a slope like ERA5, whereas the IPSL and MIROC have a slope that is too shallow, indicating that too few TCs recurve in these two models.

100

Overall, all five CMIP6 models capture the relationship between TC frequency and recurving TC frequency despite TC intensity biases, indicating that the models can capture the main driver of the interannual variability of recurving TC frequency, which may have important implications for European PTC risk.

101

102



103

104

Figure S6: Relationship between TC frequency and recurving TC frequency in ERA5 (top left) and the five selected CMIP6 models. For ERA5, data from 1979-2018 is used. For the other models, all data from the fully-coupled historical runs are used (1950-2014 for CNRM, IPSL, 1850-2014 for HadGEM, KIOST, and MIROC6). Random noise has been added to the data points so that all points can be seen, but the correlations and slopes are identified using the original data.

105

106

7. Figure 5 cyclone counts

107

Table S1 shows the PTC and MLC counts for each intensity bin in Figure 5 of the main manuscript. Note that these counts refer to the whole European domain (blue bars in Figure 5).

108

109

110

111

112

% ile bins	CNRM		HadGEM		KIOST		MIROC		IPSL	
	PTC	MLC	PTC	MLC	PTC	MLC	PTC	MLC	PTC	MLC
0-20	3	872	2	978	1	885	5	8816	14	27717
20-40	5	870	1	978	5	881	18	8802	29	27701
40-60	11	864	3	977	3	883	19	8801	47	27683
60-80	20	855	3	976	4	882	51	8769	123	27607
80-90	12	425	5	485	6	437	69	4341	94	13771
90-95	7	212	2	243	9	213	58	2147	87	6845
95+	15	204	9	236	13	209	87	2119	136	6798

113

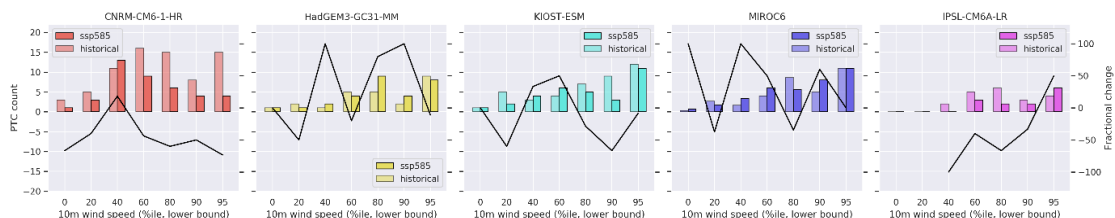
114 **Table S1. Counts for the hurricane-season-forming, Europe-impacting PTCs and MLCs shown in Figure**
115 **5 (blue bars).**

116 **8. European-impacting PTC statistics – consistent ensemble members, ensemble spread, and**
117 **additional CMIP6 models**

118 **8.1. Consistent ensemble members**

119 Finite computational resources force a compromise to be made between model resolution and length of
120 simulation/number of ensemble members. In this work, we are using relatively coarse resolution models. This
121 limitation is compensated by the large number of ensemble members available for some of the models,
122 particularly during the historical period for the MIROC6 (10) and IPSL-CM6A-IR (31). However, data is not
123 available for this many ensemble members in the future runs under the SSP585 scenario.

124 To ensure that the projected changes shown in the paper are not the result of different ensemble members being
125 considered in the historical and future periods, we repeat the analysis, this time just considering the common
126 ensemble members over the historical and future period. This is shown in Figure S7. The CNRM-CM6-1-HR,
127 HadGEM3-GC31-MM and KIOST-ESM only have one ensemble member for the historical and future period
128 and so see no change. However, for the MIROC6 we only consider the first three ensemble members for the
129 historical period (ensuring that a direct comparison can be drawn with the three ensemble members available for
130 the future period). For the IPSL-CM6A-LR, we only use the first ensemble member for the historical period, as
131 this is the only ensemble member which is available for the future period under the SSP585 scenario.



132

133 **Figure S7: As in Figure 9, but only considering common ensemble members over the historical and future**
134 **periods.**

135 There are no changes to the data (and hence results) for the CNRM, HadGEM and KIOST. When just using
 136 common ensemble members, the projected change in the number of European-impacting PTCs in the highest
 137 intensity bin is smaller (fractional change down from +20% to +5%) in the MIROC and has increased for the
 138 IPSL (fractional change up to +50% from +40%). These changes are relatively small and do not alter the key
 139 result, which is that there is no robust model response in terms of European-impacting PTC intensity changes.

140 Table S2 shows the repeated analysis for Table 2, again only considering the common ensemble members. The
 141 results are largely unchanged. All fractional changes which were shown to be significant in Table 2 (except the
 142 increase in European-impacting PTC counts in the MIROC6) are still significant when only considering
 143 common ensemble members, and therefore the robust responses seen in the models (reduction in North Atlantic
 144 TC count, increase in likelihood of recurvature) are not the result of differing ensemble sizes in the historical
 145 and future periods.

146

	N _{Europe}			N _{TC}			F _{rec}			F _{Europe rec}		
	Hist	SSP	Diff	Hist	SSP	Diff	Hist	SSP	Diff	Hist	SSP	Diff
CNRM	2.35	1.29	-45%	14.68	9.00	-39%	0.55	0.59	7%	0.29	0.24	-17%
HadGEM	0.81	0.94	16%	7.29	4.35	-40%	0.46	0.61	31%	0.24	0.35	49%
KIOST	1.32	1.03	-22%	7.97	5.19	-35%	0.41	0.40	-4%	0.40	0.50	24%
MIROC	1.08	1.17	8%	8.37	5.53	-34%	0.43	0.68	58%	0.30	0.31	3%
IPSL	0.65	0.42	-35%	8.84	3.16	-64%	0.20	0.42	110%	0.36	0.32	-11%

147

148 **Table S2: As in Table 2, but only considering common ensemble members between the historical and**
 149 **future periods.**

150 While there are some differences between results produced using all ensemble members and common ensemble
 151 members, they do not differ significantly, and they do not change the results of the paper.

152 8.2. Ensemble spread

153 The analysis of section 8.1 shows that the key results of the main manuscript are not sensitive to whether or not
 154 common ensemble members are used between the historical and future periods. This subsection investigates the
 155 ensemble spread in the cyclone statistics of Table 2 (main manuscript) in the two models for which multiple
 156 ensemble members are available, MIROC and IPSL.

157 Table S3 shows the cyclone statistics from Table 2 in the main manuscript, along with the proportion of TCs
 158 reaching Europe as PTCs ($= F_{rec}F_{Eur|rec}$) for the MIROC and IPSL. Instead of combining all ensemble members
 159 before the calculation of the statistics, here the statistics are calculated for each ensemble member individually
 160 and the minimum and maximum ensemble members are shown for each of the statistics.

161 While there is a large spread amongst ensemble members for MIROC and IPSL for both time periods, the
 162 ensemble spread is considerably smaller than the projected change in North Atlantic TC frequency (N_{TC}), the
 163 fraction of recurving TCs (F_{Rec}) and the fraction of North Atlantic TCs reaching Europe (F_{Rec}F_{Eur|Rec}).

	MIROC (10, 3)		IPSL (31, 1)	
	Hist	SSP	Hist	SSP
N_{TC}	(7.26, 8.29)	(5.23, 6.0)	(7.42, 8.84)	3.16
F_{rec}	(0.37, 0.49)	(0.66, 0.71)	(0.16, 0.23)	0.42
$F_{Europe rec}$	(0.23, 0.36)	(0.31, 0.32)	(0.18, 0.44)	0.32
N_{Europe}	(0.74, 1.29)	(1.06, 1.23)	(0.26, 0.65)	0.42
$F_{rec} F_{Europe rec}$	(0.09, 0.16)	(0.20, 0.23)	(0.03, 0.08)	0.13

164

165 **Table S3. Values of the ensemble minimum and maximum (min, max) North Atlantic TC frequency (row**
166 **2), fraction of recurring TCs (row 3), fraction of recurring TCs reaching Europe (row 4), Europe-**
167 **impacting PTC frequency (row 5) and fraction of North Atlantic TCs reaching Europe (row 6) for**
168 **MIROC (columns 2, 3) and IPSL (columns 4, 5) in the historical and future simulations. The number of**
169 **available ensemble members in MIROC and IPSL are given in brackets in row 1.**

170 8.3. Additional CMIP6 models

171 This subsection investigates the cyclone statistics shown in Table 2 of the main manuscript, along with the
172 projected change in the fraction of North Atlantic TCs reaching Europe as PTCs, in 10 additional CMIP6
173 ScenarioMIP models for which sufficient data is available for cyclone tracking and TC identification. These
174 additional models were not selected for use in the main manuscript as they do not simulate North Atlantic TC
175 frequency reasonably compared to observations and reanalyses but are briefly investigated here with the aim of
176 identifying any robust projected changes. TCs in the additional 10 CMIP6 models are identified using the same
177 tracking scheme and TC identification method. The same time periods (1984-2014 and 2069-99) and future
178 scenario (SSP5-85) are also used. The additional 10 CMIP6 models are shown in Figure S1 (blue shading).

179 The results of Table S4 are consistent with the results presented for the five selected models in the main
180 manuscript (Table 2). 9 of the 10 additional CMIP6 models project a significant decrease in North Atlantic TC
181 frequency. All 10 models have a projected increase in the fraction of recurring TCs, significant in 4 models. The
182 proportion of North Atlantic TCs reaching Europe as PTCs (Table S5) is projected to increase in 7 of the 10
183 additional models, significantly in 4. EC-Earth3 is a significant outlier compared to the wider model ensemble.
184 In this model, North Atlantic TC frequency and the fraction of recurring TCs are both projected to increase,
185 leading to a significant increase in projected Europe-impacting PTC frequency.

186 This additional analysis highlights the robust projected decrease in North Atlantic TC frequency, which is offset
187 to some extent by an increase in the likelihood that a TC will reach Europe in CMIP6 models.

	N_{TC}			F_{rec}			$F_{Europe rec}$			N_{Europe}		
	Hist	SSP	Diff	Hist	SSP	Diff	Hist	SSP	Diff	Hist	SSP	Diff
ACCESS-CM2	104	49	-53%	0.41	0.71	73%	0.35	0.43	23%	15	15	0%
BCC-CSM2-MR	109	60	-45%	0.53	0.57	6%	0.34	0.29	-15%	20	10	-50%
EC-Earth3	45	65	47%	0.44	0.62	41%	0.32	0.37	14%	6.3	14.9	133%
MIROC-ES2L	16	4	-73%	0.31	0.75	139%	0.31	0	-100%	1.5	0	-100%

MPI-ESM1-2-HR	61	33	-47%	0.25	0.34	33%	0.30	0.32	7%	4.6	3.5	-25%
MPI-ESM1-2-LR	48	27	-44%	0.33	0.37	13%	0.34	0.34	-1%	5.4	3.4	-40%
MRI-ESM2-0	153	45	-70%	0.49	0.73	51%	0.30	0.39	30%	22.4	13	-41%
NESM3	146	74	-49%	0.46	0.69	50%	0.28	0.35	25%	19	18	-5%
NorESM2-LM	77	58	-25%	0.52	0.59	14%	0.40	0.44	9%	16	15	-6%
NorESM2-MM	169	73	-57%	0.49	0.52	7%	0.41	0.32	-24%	34	12	-64%

188

189 **Table S4. As in Table 2 of the main manuscript, but for 10 additional (and poorer-performing with**
190 **respect to North Atlantic TC frequency) CMIP6 ScenarioMIP models.**

191

192

	Proportion of TCs reaching Europe (= $F_{rec} F_{Europe rec}$)		
	Hist	SSP	Diff
ACCESS-CM2	0.14	0.31	122%
BCC-CSM2-MR	0.18	0.17	-9%
EC-Earth3	0.14	0.23	61%
MIROC-ES2L	0.10	0.0	-100%
MPI-ESM1-2-HR	0.08	0.11	42%
MPI-ESM1-2-LR	0.11	0.13	12%
MRI-ESM2-0	0.15	0.29	97%
NESM3	0.13	0.24	87%
NorESM2-LM	0.21	0.26	24%
NorESM2-MM	0.20	0.16	-18%

193

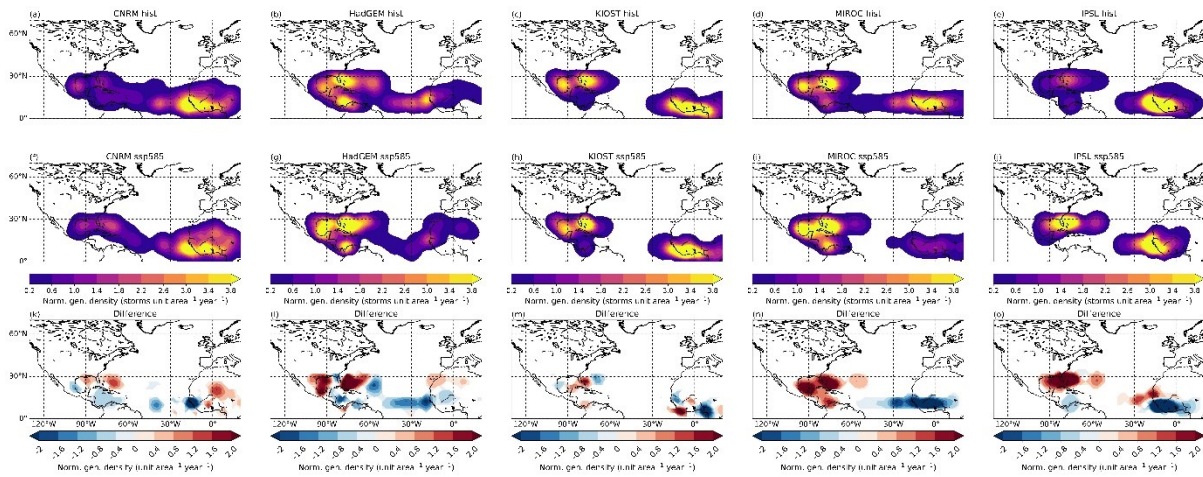
194 **Table S5. Proportion of North Atlantic TCs reaching Europe in the historical (1984-2014) and future**
195 **(2069-99) period under the SSP5-85 scenario (columns 2 and 3 respectively). Fractional change in shown**
196 **in column 4. Bolded differences represent statistical significance at the 95% level using a bootstrap**
197 **resampling method.**

198

9. Normalized genesis density changes

199 Figure S8 shows the change in the normalized genesis density in the five CMIP6 models. There is a robust
200 model response for a shift in genesis (proportionally) away from the MDR towards the WEST and SUB regions.
201 This difference is largest in the HadGEM, MIROC and IPSL - the three models in which there is the largest
202 increase in the likelihood of recurvature - and is consistent with the results of Table 3.

203



205

206 **Figure S8: Normalized genesis density for the 5 selected CMIP6 models during the historical (top) period,**
 207 **towards the end of the century under SSP585 (middle), and the difference (future minus historical,**
 208 **bottom). Densities less than 0.2 have been masked for clarity.**

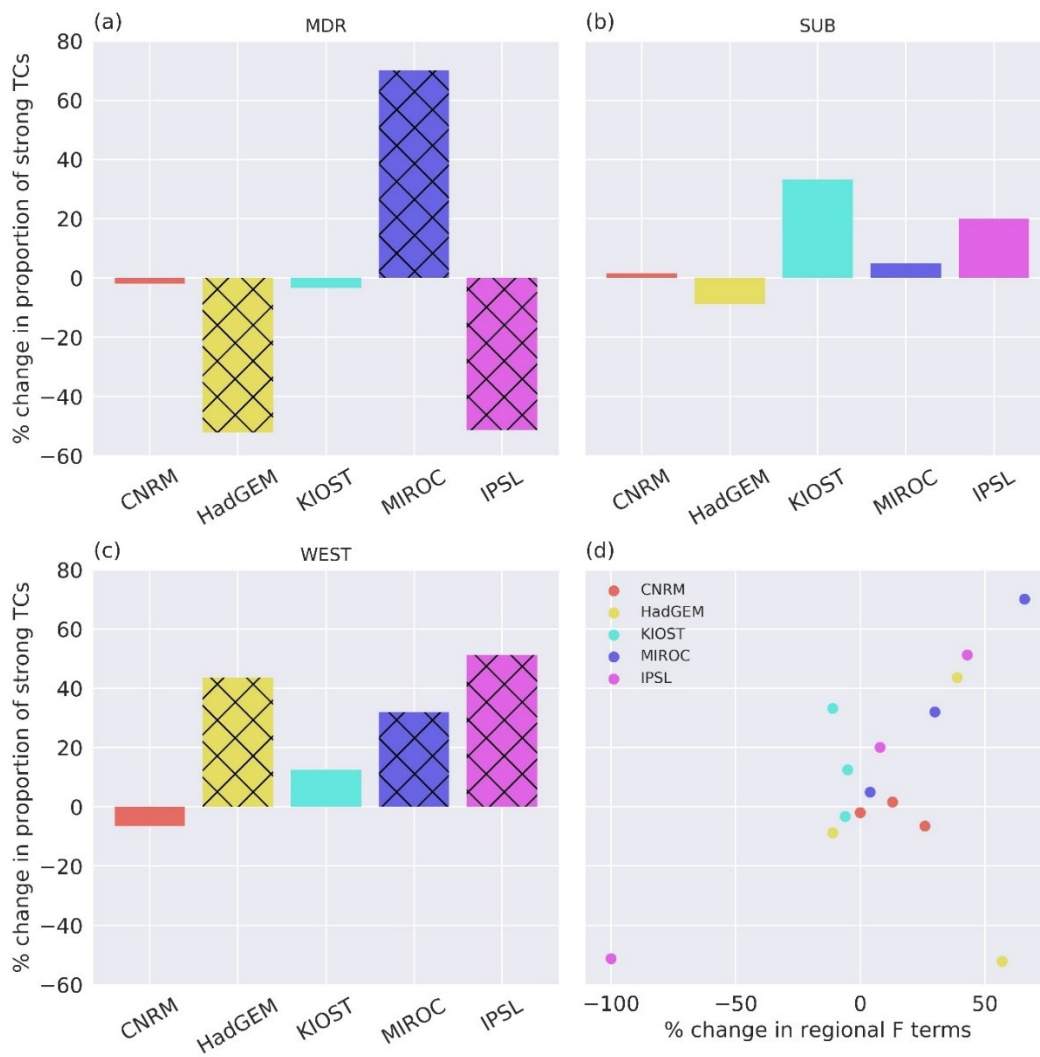
209

210 10. TC LMI changes

211 While shifts in genesis explain most of the projected change in F_{Rec} in HadGEM, MIROC and IPSL, they do not
 212 explain all of the projected increase. To further investigate the projected changes in F_{Rec} , the relationship
 213 between projected TC LMI changes and projected F_{Rec} changes is explored. Figure S9 shows the change in TC
 214 LMI for the 5 selected models, for each of the three regions in equation (3) and Table 3 (main manuscript),
 215 along with a scatterplot of TC LMI changes against recurvature likelihood changes within the regions.

216 In the MDR, there is a large increase in the proportion of North Atlantic TCs which are strong (TC LMI > mean
 217 of the combined (historical + future) North Atlantic TC distribution) in MIROC. In the WEST region, this is
 218 also true for HadGEM, MIROC and IPSL. These are also the only four models/regions in our selection of
 219 CMIP6 models where there is a statistically significant increase in the likelihood of recurvature (Table 3, main
 220 manuscript). Figure S9d shows a strong relationship between TC LMI changes and changes in recurvature
 221 likelihood within regions. It is therefore possible that changes in TC LMI – particularly in the WEST regions of
 222 MIROC, HadGEM and IPSL, and MDR of MIROC – are associated with the projected increase in F_{Rec} . For Fig.
 223 S9d, the Pearson's correlation coefficient is 0.52 and is significant at the 95% level. However, it should be noted
 224 that this is only a correlation over 15 data points. It is not completely clear from the GPI (Fig. 6) why the TC
 225 LMI is seen to increase in the WEST regions in HadGEM and IPSL, and the MDR and WEST regions in
 226 MIROC.

227



228

229 **Figure S9: Bar charts showing the percentage change in the proportion of strong North Atlantic TCs**
 230 **(TCs which have a TC LMI greater than the mean of the combined (historical + future) distribution) in**
 231 **the MDR (a), SUB (b) and WEST (c) regions. (d) shows a scatterplot of the percentage change in the**
 232 **proportion of strong North Atlantic TCs against the percentage change in the F terms within the**
 233 **individual regions (columns 3, 5, and 7 of the bottom of Table 3, main manuscript). Hatching represents**
 234 **the models and regions in which the % change is significant to 95% using a bootstrapping method.**

235

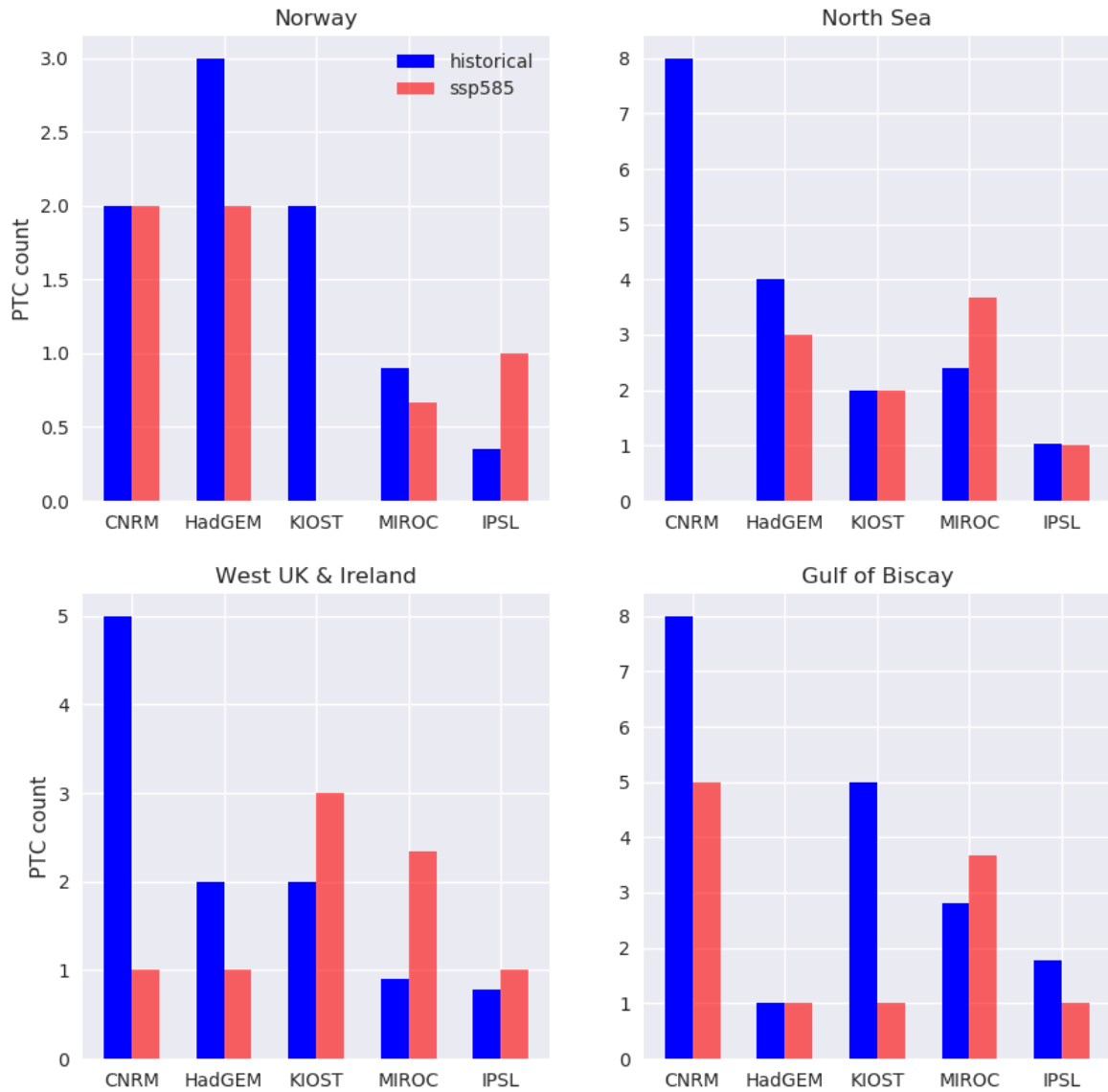
236 **11. Direct comparison with Haarsma et al. (2013)**

237 The only previous studies which investigate projected changes in European-impacting PTCs find a large
 238 increase in the number of high-intensity PTCs in the future (Haarsma et al. 2013, hereafter H13; Baatsen et al.
 239 2015). None of the CMIP6 models investigated in this study show an increase as large as found in these
 240 previous studies (driven by a very large decrease in TC counts basin-wide). However, the results presented in
 241 section 3.2. do not use the same methodology as used in H13.

242 To make our work as comparable as possible to H13, the analysis of Figures 9 and 10 are repeated with some
243 methodological changes. As in H13, we only consider cyclones which impact Europe (Fig. S10) or form (Figs
244 S11, S12) during August, September, and October. We also change the domain of interest to look at the same
245 four regions which were used in H13: Norway (60-70N, 0-15E), North Sea (50-60N, 3W-8E), Western UK and
246 Ireland (50-60N, 3-15W) and the Gulf of Biscay (43-50N, 0-15W).

247 Due to the lower resolution of the CMIP6 models than used in H13, we cannot use the same intensity threshold
248 of hurricane force ($>33\text{ms}^{-1}$) winds. We instead just consider cyclones impacting each of the four regions in
249 ASO which have maximum winds in the region greater than the 90th percentile of the combined (PTC+MLC,
250 historical + future) distribution of cyclone maximum winds in the region. This gives us a similar PTC frequency
251 as in H13 (Fig 2f therein).

252 Figure S10 shows mixed changes in the number of strong PTCs impacting each region in the future, though
253 more regions and models project decreases than increases. Sample sizes are extremely small, as the Europe sub-
254 regions are considerably smaller than the European domain used in the main manuscript. The result of Figure
255 S10 is different from the result of H13, in which there was a substantial increase in strong PTCs in the future
256 across three of these four regions. However, when considering the fraction of North Atlantic TCs forming in
257 ASO which impact each of these regions (Figure S11 for all PTCs, Figure S12 for strong PTCs ($> 90^{\text{th}}$
258 percentile)), there's a general increase, in line with Figure 10 from the main manuscript. This suggests that in
259 the future, North Atlantic TCs are more likely to reach these four regions of Europe, and future risk to these
260 regions depends strongly on the projected change in basin-wide TC counts.



261

262 **Figure S10: Number of high intensity PTCs (max wind in region > 90th percentile of combined**
 263 **distribution) impacting each of the four regions during Aug-Oct in the historical period (blue) and future**
 264 **period under the SSP585 scenario (red).**

265

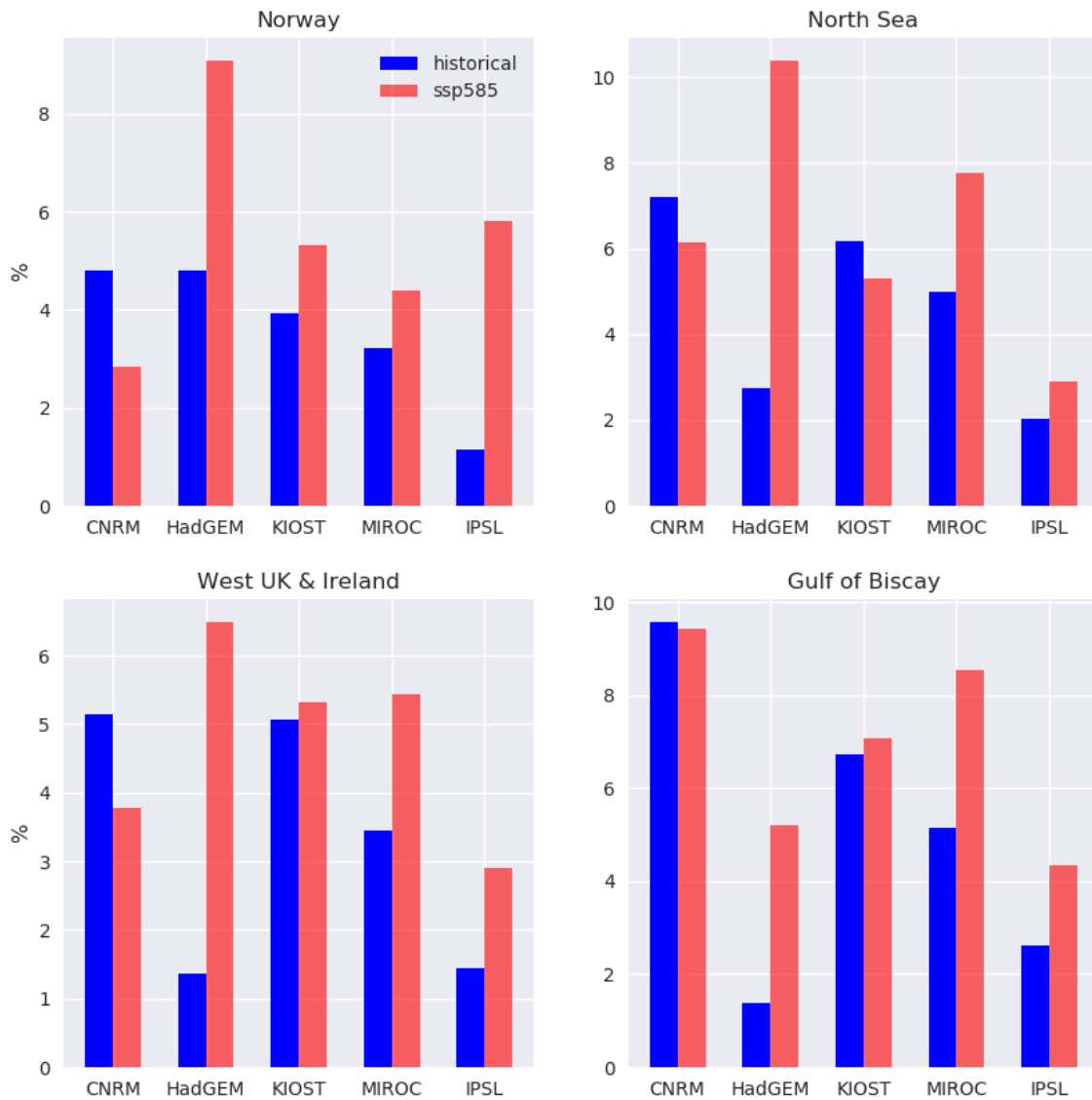
266

267

268

269

European-impacting PTCs



270

271 **Figure S11: Fraction of North Atlantic TCs which impact the given four regions as PTCs, considering all**
 272 **North Atlantic TCs forming during August-October in the historical period (blue) and future period**
 273 **under the SSP585 scenario (red).**

274

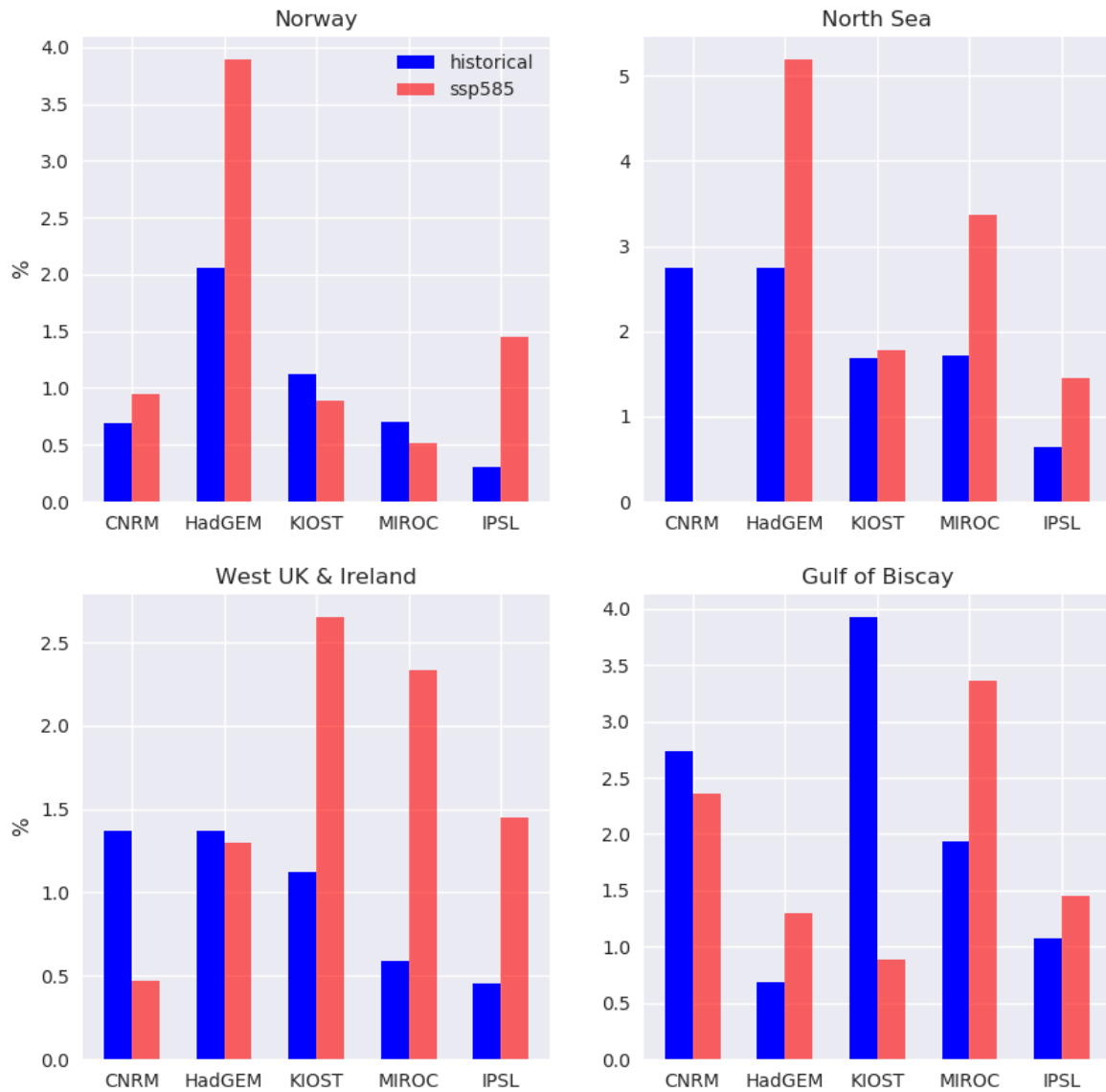
275

276

277

278

strong PTCs: > 90th %ile



279

280 **Figure S12: As in Figure S11 but considering the fraction of North Atlantic TCs which reach the four**
281 **regions as strong PTCs (winds > 90th percentile of the max wind distribution in the region).**

282